

Fermi Volume Evolution and Crystal-Field Excitations in Heavy-Fermion Compounds Probed by Time-Domain Terahertz Spectroscopy

S. Pal,¹ C. Wetli,¹ F. Zamani,² O. Stockert,³ H. v. Löhneysen,⁴ M. Fiebig,^{1,*} and J. Kroha^{2,5,†}

¹*Department of Materials, ETH Zürich, 8093 Zürich, Switzerland*

²*Physikalisches Institut and Bethe Center for Theoretical Physics, Universität Bonn, Nussallee 12, 53115 Bonn, Germany*

³*Max Planck Institute for Chemical Physics of Solids, 01187 Dresden, Germany*

⁴*Institut für Festkörperphysik and Physikalisches Institut, Karlsruhe Institute of Technology, 76021 Karlsruhe, Germany*

⁵*Center for Correlated Matter, Zhejiang University, Hangzhou, Zhejiang 310058, China*

(Dated: March 7, 2019)

We measure the quasiparticle weight in the heavy-fermion compound $\text{CeCu}_{6-x}\text{Au}_x$ ($x = 0, 0.1$) by time-resolved terahertz spectroscopy for temperatures from 2 up to 300 K. This method distinguishes contributions from the heavy Kondo band and from the crystal-electric-field satellite bands by different terahertz response delay times. We find that the formation of heavy bands is controlled by an exponentially enhanced, high-energy Kondo scale once the crystal-electric-field states become thermally occupied. We corroborate these observations by temperature-dependent dynamical mean-field calculations for the multiorbital Anderson lattice model and discuss consequences for quantum-critical scenarios.

In heavy-fermion materials [1], a lattice of rare-earth ions with local magnetic moments in the $4f$ shell is embedded in a metallic host. With decreasing temperature, the Kondo effect drives part of the $4f$ spectral weight to the Kondo resonance near the Fermi energy ε_F [2] where it forms a band of lattice-coherent, heavy quasiparticles (QPs). Consequently, part of the $4f$ electrons become itinerant, and the Fermi volume expands so as to accommodate the extra number of indistinguishable $4f$ electrons in the Fermi sea. The existence of an enlarged Fermi volume is, therefore, a unique signature of the Kondo-induced heavy Fermi-liquid phase, its absence a signature of heavy-QP destruction [3, 4], as it may occur, e.g., near a quantum phase transition (QPT) [5–7]. Within the standard Anderson lattice model, the crossover energy scale above which the Kondo correlations fade away is the Kondo lattice temperature T_K^* . However, the recent observation of a large Fermi surface in the heavy-fermion compound YbRh_2Si_2 at temperatures $T \gg T_K^*$ by angle-resolved photoemission spectroscopy (ARPES) [8] has raised disputes about this picture [4, 8–10]. In particular, it has been questioned whether T_K^* , as extracted from low-temperature thermodynamic and transport measurements, is the correct scale for heavy-QP formation, or whether they can persist to much higher energies [8]. This question is important, because the behavior of the QP formation scale near a heavy-fermion QPT is a hallmark distinguishing different quantum-critical scenarios, like the spin-density-wave scenario [11–13], the local quantum-critical scenario [5, 14], or other schemes of QP destruction [15–17].

In this Letter, we resolve this puzzle by separately measuring the Kondo and the crystal-electric-field (CEF) contributions to the Fermi volume using time-resolved terahertz spectroscopy [18] and temperature-dependent dynamical mean-field theory (DMFT) calculations. Time-domain terahertz spectroscopy has been recently developed

as a method particularly sensitive to the QP dynamics in strongly correlated electron systems [18]. We find that for the heavy-fermion compound $\text{CeCu}_{6-x}\text{Au}_x$, the spectral weight contributing to the large Fermi volume at high temperatures is accounted for by the CEF satellite resonances of the Ce $4f$ orbitals, while the low-temperature behavior is controlled by the Kondo resonance, in particular near the QPT at $x = 0.1$. This reconciles the seemingly contradictory ARPES results [8].

CEF resonances.—CEF satellite structures in heavy-fermion systems have been previously observed by photoemission [19–21] and scanning tunneling [22, 23] spectroscopy. In order to understand their impact, one must realize that CEF resonances originate from the same strong correlation effect that generates the low-energy Kondo resonance itself [20, 24]. In the orthorhombic lattice structure of $\text{CeCu}_{6-x}\text{Au}_x$, the $j = 5/2$ ground-state multiplet of the Ce $4f$ orbitals is split by the CEF into three Kramers doublets, denoted by $\varepsilon_0, \varepsilon_1, \varepsilon_2$ (see Fig. 1). Only one of the CEF states is significantly occupied at any time due to strong Coulomb repulsion within the Ce $4f$ orbitals. By the hybridization of these orbitals with the conduction-electron states, a Ce $4f$ electron can fluctuate from the ground-state Kramers doublet ε_0 into a conduction state near ε_F and back to ε_0 , shown as process (0) in Fig. 1. This process involves spin exchange with the conduction electrons and is quasielastic (final and initial energies are equal, ε_0), i.e., in resonance with the low-energy conduction electron states [25, 26]. The singular quantum spin-flip scattering thus generates the narrow Kondo resonance in the Ce $4f$ spectrum at ε_F , shown as peak (0) in Fig. 1. Alternatively, the $4f$ electron can end up in one of the CEF-excited levels, ε_m ($m = 1, 2$) instead of ε_0 [process (1) in Fig. 1]. Involving again singular quantum spin-flip transitions, this process generates another narrow resonance, albeit shifted in energy by the final-state excitation energy

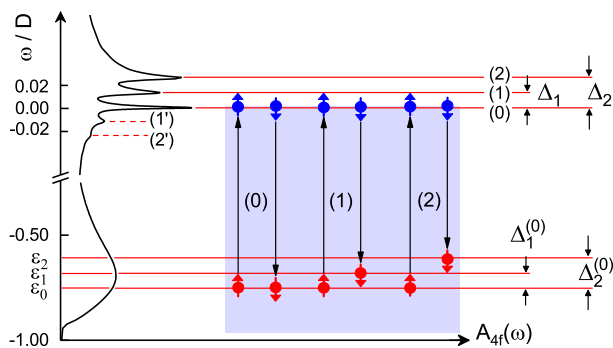


Figure 1. Ce $4f$ spectral density for $T \ll T_K^* < \Delta_1$ (black curve) as calculated by DMFT for CeCu₆. The long arrows represent the hybridization processes between Ce $4f$ electrons (red) and conduction electrons (blue dots and shaded region) generating the Kondo and CEF resonances. The energy scale around the Fermi energy ($\omega=0$) is stretched by a factor 5.

$\Delta_m = \varepsilon_m - \varepsilon_0 + \delta\Delta_m$, i.e., by the bare CEF excitation energy $\Delta_m^{(0)} = \varepsilon_m - \varepsilon_0$ and additional many-body renormalizations $\delta\Delta_m$ [peak (1) in Fig 1]. For each of the CEF satellites (1), (2) there exists a mirror satellite (1'), (2') [19, 20, 24] shifted downward by $-\Delta_m$, see Fig. 1. The mirror satellites appear as weak peaks or shoulders only, because they originate from transitions $\varepsilon_{1,2} \rightarrow \varepsilon_0$ whose initial states $\varepsilon_{1,2}$ have only a small, albeit nonzero (due to hybridization with the conduction band) virtual population even at $T \ll \Delta_1$. From the above discussion, it is clear that the CEF satellite resonances are of spin-scattering origin, just like the Kondo resonance itself. Thus, for $k_B T_{K,m} \lesssim k_B T \ll \Delta_1$ their weight has a logarithmic temperature dependence, and their width is renormalized by many-body effects to exponentially small values of $T_{K,m} \approx D \exp[-1/(2N_F J_m)]$ [2, 24], where D is the conduction half bandwidth, N_F the (unrenormalized) density of states at the Fermi level, and J_m the effective spin exchange coupling of the conduction electrons with the CEF level $m = 0, 1, 2$, up to higher-order renormalizations [20, 24]. In fact, this narrow width makes the CEF satellite resonances energetically separated and resolvable in spectroscopic experiments [19, 20, 22] for $k_B T \ll \Delta_1$, while the hybridization width of the single-particle levels $\varepsilon_0, \varepsilon_1, \varepsilon_2$ is orders of magnitude larger than their splitting $\Delta_m^{(0)}$, see Fig. 1. As the temperature is raised to $k_B T \approx \Delta_1$, at least one of the CEF-excited satellites becomes thermally occupied and acts as effectively degenerate levels, leading to the effective high-temperature Kondo scale $T_K^{(\text{high})} \approx D \exp[-1/(2N_F \sum'_m J_m)]$, where the sum \sum'_m runs over the CEF levels m with significant thermal occupation.

To quantify this behavior, we performed DMFT calculations for the multiorbital Anderson lattice model with three local levels ε_m , corresponding to the three Kramers doublets of the $j = 5/2$ Ce $4f$ ground-state multiplet in CeCu₆. The near-single occupancy of the Ce $4f$ shell was enforced by a strong interlevel repulsion, $U \rightarrow \infty$. We chose the

bare model parameters such that the DMFT produces the values for T_K^* and the CEF splittings reported in the literature [21, 27–29] (see [30] for details). The resulting DMFT spectra $A_{4f}(\omega)$ in Fig. 3 (a) exhibit the crossover from the high-temperature scale $T_K^{(\text{high})} \approx 200 \text{ K} \hat{=} 17 \text{ meV}$ to the low-energy Kondo scale $T_K^* = T_{K,0} \approx 6 \text{ K} \hat{=} 0.52 \text{ meV}$.

Time-resolved terahertz spectroscopy.—We investigate the temperature dependence of the QP spectral weight in the CeCu_{6-x}Au_x system. CeCu₆ has a Kondo lattice scale of $T_K^* \approx 6 \text{ K}$ and CEF excitations at $\Delta_1 = 7 \text{ meV}$ and $\Delta_2 = 13 \text{ meV}$ [27–29]. CeCu_{6-x}Au_x undergoes a magnetic QPT at $x = 0.1$ [1]. We generate terahertz pulses of 1.5 cycles duration, covering a frequency range of 0.1–3 THz, by optical rectification in a 0.5 mm (110)-oriented ZnTe crystal. We radiate these pulses onto samples of the Fermi-liquid compound CeCu₆ and of the quantum-critical compound CeCu_{5.9}Au_{0.1} (see [30] for details). The terahertz radiation induces symmetry-allowed dipole transitions from the CEF-split heavy-fermion bands to the light band of Ce $5d$ –Cu $4s$ character. The reflected terahertz electric field is detected via free-space electro-optic sampling on a 0.5 mm (110)-oriented ZnTe crystal that is optically bonded to a 2 mm (100)-oriented ZnTe crystal. In this way, time traces of the reflected signal are taken from $t = -4 \text{ ps}$ to $+8.5 \text{ ps}$ in steps of 0.04 ps. All time traces are normalized by a factor such that the integrated intensity equals one, representing identical total reflected power. It has been shown previously [18] that a correlated many-body state manifests itself in the reflected terahertz electric field as a temporally confined and delayed pulse whose delay time resembles the QP lifetime (inverse spectral width), its integrated weight the QP weight. In particular, for a band of heavy Kondo QPs with spectral width $k_B T_K^*$ the delay time is $\tau_K^* = h/k_B T_K^*$, with h the Planck constant and k_B the Boltzmann constant [18]. The temporally delayed pulse thus provides a direct and background-free probe for the QP dynamics of strongly correlated states.

Analysis of spectral features.—A terahertz signal reflected from a CeCu₆ sample is shown in Fig. 2 (a) in comparison to a platinum reference signal. It exhibits three distinct features labeled (i), (ii), (iii). We note that other features visible are statistical fluctuations: They show no systematic temperature dependence and average out over ten measurements. In the time interval $[-2.5 \text{ ps}, +2.5 \text{ ps}]$ the signal consists of two overlapping features (i) and (ii). The strong, instantaneous pulse (i) centered at $t = 0 \text{ ps}$ appears almost identically in CeCu₆ and in Pt and is temperature independent [not shown in Fig. 2 (a)]. It is the stimulated single-particle response of the light conduction electrons. In addition, there is a weaker feature (ii) visible as the wiggles superimposed on the wing of pulse (i). We observe that this signal does not appear in the Pt reference, has a reproducible, nonmonotonic temperature dependence (analyzed below), and vanishes in all measured time traces below $T = 5 \text{ K}$. We use this temperature dependence to separate signal (ii) from the single-particle reflex (i): We

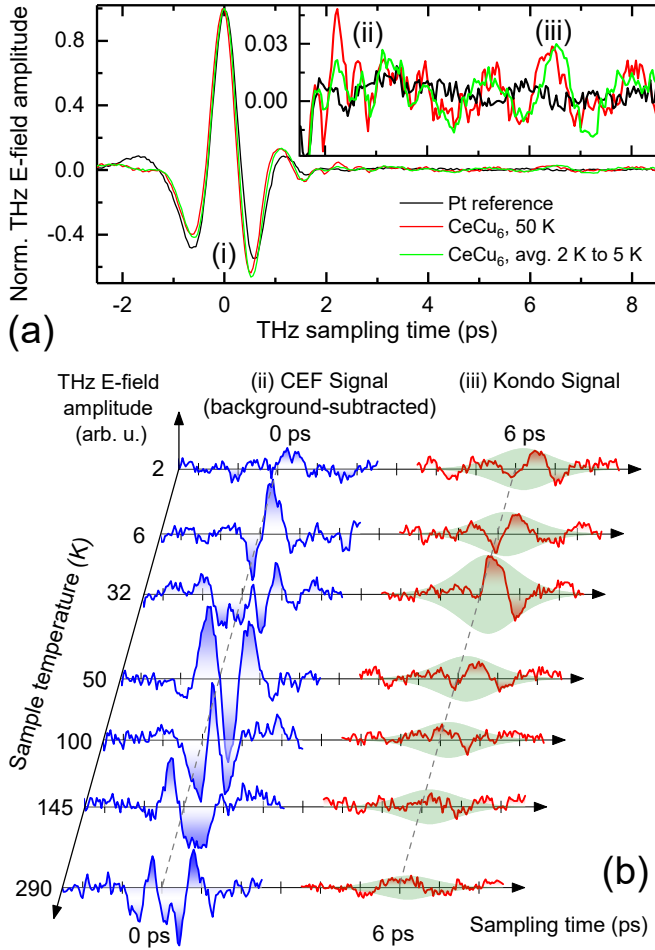


Figure 2. (a) Time traces of the terahertz electric field reflected from a CeCu_6 sample at $T = 50$ K (red) in comparison to a Pt reference at $T = 2.0$ K (black) and the average of the CeCu_6 time traces for temperatures between 2.0 and 5.0 K (green). (b) Evolution of the background-subtracted CEF signal (-2.5 to $+2.5$ ps) and the Kondo signal ($+3.5$ to $+8.5$ ps) as the temperature decreases from 290 to 2 K. The green-shaded region depicting the envelope of the Kondo signal is a solution of the nonlinear rate equation of Ref. [18] describing the relaxation of the terahertz-excited heavy-fermion system with a single local orbital. Trivial delayed reflexes originating from the terahertz generation crystal or the cryostat windows have been identified at times $t > 10$ ps [18].

take the temperature average of the time traces taken between 2 and 5 K and subtract it from each time trace within the time interval $[-2.5$ ps, $+2.5$ ps]. Finally, the pulse (iii), centered around 6 ps, has been identified earlier [18] with the Kondo resonance by its characteristic temperature dependence [c.f. Fig. 2(b)] and by its delay time agreeing well with the Kondo QP lifetime τ_K^* . For the detailed analysis of this signal, see Ref. [18].

The resulting, correlation-induced and background-subtracted time traces are shown in Fig. 2(b). The amplitude of the signal (iii) from the heavy Kondo band rises with decreasing temperature and remains finite at the low-

est temperatures, with some decrease due to the vicinity of the QPT [18]. The background subtraction reveals that the reflex (ii) is not only located around 2 ps, but also extends over a wider time range centered around the short delay time of $\tau_{\text{CEF}} \approx 0.25$ ps. It also rises with decreasing temperature, but reaches a maximum near $T = 60$ K and then decreases to undetectably small values for $T \lesssim 5$ K. Such nonmonotonic behavior is a clear signature of the CEF resonances, as can be seen from the DMFT calculations of Fig. 3(a): On reducing the temperature, a single, broad resonance of width $\Gamma_{\text{CEF}} = k_B T_K^{(\text{high})} \approx 17$ meV rises up, corresponding to the increase of the signal (ii) in Fig. 2 (b). Below about 60 K the broad resonance in Fig. 3 (a) splits into three individual, sharp CEF peaks of which only the lowest one is occupied towards $T = 0$. Correspondingly, the short-delayed signal (ii) in Fig. 2 (b) disappears, and part of its weight reappears in the Kondo pulse (iii) with $\tau_K^* = h/k_B T_{K,0} = h/k_B T_K^* = 6$ ps delay time. Hence, we have unambiguously associated the time traces (ii) in Fig. 2 (b) to the broad CEF resonance of Fig. 3 (a).

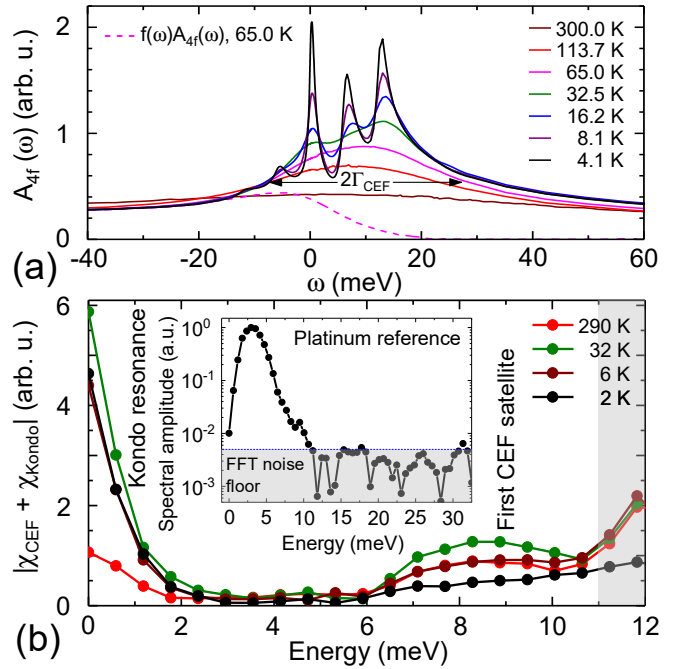


Figure 3. (a) Temperature dependence of the momentum-integrated Ce $4f$ spectral density in CeCu_6 (solid lines), as calculated by DMFT for the Anderson lattice model. The occupied spectral density at 65.0 K, $f(\omega) A_{4f}(\omega)$ (dashed line; $f(\omega)$ is the Fermi-Dirac distribution), visualizes that the spectral width, $\Gamma_{\text{CEF}} = k_B T_K^{(\text{high})} \approx 17$ meV $\hat{=} 200$ K, is not accounted for by thermal broadening at 65.0 K alone. (b) Magnitude spectrum of the CEF and Kondo responses of CeCu_6 . The Kondo response peaks near zero energy, and has a width of 0.56 meV ($\hat{=} 6.7$ K) which agrees very well with $k_B T_K^*$. The first CEF satellite is seen at 8 meV, close to the literature value [27–29]. The shaded region is beyond the spectral width of the terahertz excitation, i.e., governed by noise. The inset shows the Pt reference, equivalent to the incident terahertz spectrum $|E_{\text{in}}(\omega)|$.

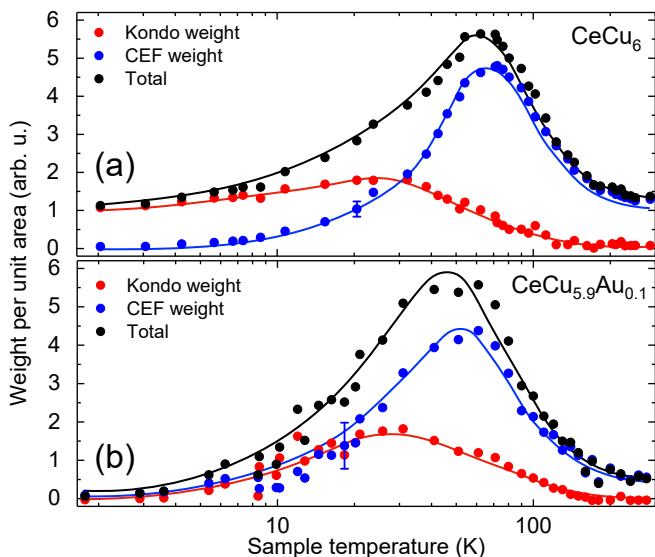


Figure 4. Temperature dependence of the occupied weights of the Kondo (red) and of the CEF (blue) bands as well as the sum of the two (black) for (a) CeCu_6 and (b) $\text{CeCu}_{5.9}\text{Au}_{0.1}$. The error bars result from averaging over ten measurements for each data point.

Further evidence for the CEF satellites is provided from the spectral analysis using the (nonequilibrium) response function $\chi(\omega) = E_{\text{out}}(\omega)/E_{\text{in}}(\omega)$, defined as the ratio of the Fourier transforms of the reflected signal $E_{\text{out}}(\omega)$ and the incident light pulse $E_{\text{in}}(\omega)$ (given by the Pt reference in the present case). The magnitude spectrum of the sum of the response functions $\chi_{\text{CEF}}(\omega)$ and $\chi_{\text{Kondo}}(\omega)$ resulting from the traces (ii) and (iii) of Fig. 2 (b), respectively, is shown in Fig. 3 (b). It clearly exhibits the Kondo resonance and the first CEF satellite resonance, including their characteristic temperature dependences.

Large Fermi volume at high temperatures.—We can now separately analyze the Fermi volume change induced by the low-temperature Kondo effect and by the CEF excitations. We integrate, after background subtraction, the time traces of the squared terahertz electric field over the time intervals $[-2.5 \text{ ps}, +2.5 \text{ ps}]$ (ii) and $[+3.5 \text{ ps}, +8.5 \text{ ps}]$ (iii) in Fig. 2 (b). The weights calculated in this way represent directly the total occupation numbers of the heavy Kondo and CEF satellite bands near ε_F , respectively, since the terahertz excitation is sensitive to occupied states only. Thus, these weights directly account for the correlation-induced Fermi volume change [33, 34]. The temperature-dependent results are shown for CeCu_6 in Fig. 4 (a). The Kondo as well as the CEF weights rise logarithmically with decreasing temperature, confirming their Kondo-like origin. The Kondo weight reaches a maximum near $T = 30 \text{ K}$ and settles to a finite value at the lowest temperatures. The CEF weight dominates the high-temperature behavior up to a characteristic temperature of $T_K^{(\text{high})} \approx 200 \text{ K} \cong 17 \text{ meV}$, read off from the onset of its logarithmic rise and in good quantitative agreement with the DMFT result for the CEF

resonance width at high temperature [Fig. 3 (a)]. The CEF weight vanishes gradually below $\sim 60 \text{ K}$, when the CEF satellite occupation gets frozen out and is transferred to the rising Kondo weight. The smooth crossover is confirmed by the momentum-resolved DMFT calculations, shown in Fig. 5. It is in line with ARPES results on other heavy-fermion compounds [10, 35, 36]. Thus, our experimental findings and theoretical calculations reveal consistently that an enlarged Fermi volume persists at temperatures much higher than T_K^* due to the CEF satellite contributions, but it is carried by the Kondo spectral weight alone when the temperature is lowered below the CEF splitting Δ_1 . The results of analogous measurements for the quantum-critical compound $\text{CeCu}_{5.9}\text{Au}_{0.1}$ are shown in Fig. 4 (b). We see that the CEF contribution to the Fermi volume is almost identical to that in the Fermi-liquid compound CeCu_6 for all temperatures. However, the Kondo spectral weight is seen to vanish at the quantum-critical point in $\text{CeCu}_{6-x}\text{Au}_x$.

Conclusion.—Time-domain THz spectroscopy provides a nearly background-free probe of quasiparticle dynamics in correlated electron systems with a characteristic energy scale in the terahertz range. Our measurements and DMFT calculations on $\text{CeCu}_{6-x}\text{Au}_x$ show that the spectral weight near the Fermi level is governed by a heavy-quasiparticle state whose width crosses over from the CEF-induced high-energy scale $T_K^{(\text{high})}$ to the Kondo lattice scale T_K^* at low temperature. Terahertz reflection acts as a “time filter” separating the CEF excitations from the Kondo resonance

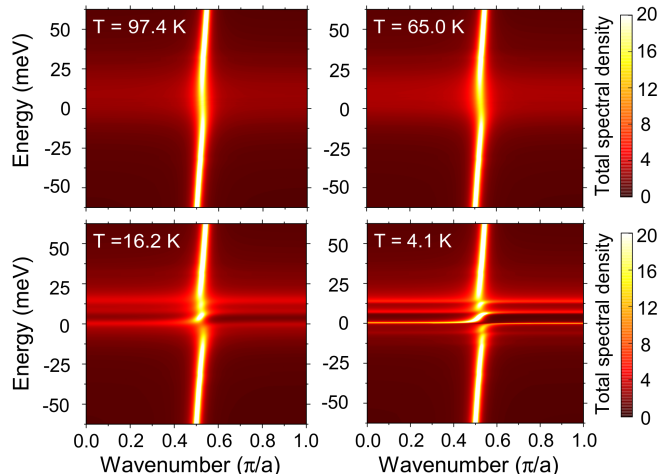


Figure 5. DMFT band structure near ε_F of a three-orbital Anderson lattice for several temperatures. The model parameter values are chosen in order to resemble CeCu_6 , $T_K^* \approx 6 \text{ K}$ and $\Delta_1 = 7 \text{ meV}$, $\Delta_2 = 13 \text{ meV}$. The nearly vertical line represents the light conduction band. At low temperatures, $T \lesssim T_K^*$, the sharp, heavy Kondo and CEF satellite bands are well resolved, each one hybridizing with the conduction band. At high temperatures, $T \gtrsim \Delta_1$, they merge to a single, heavy band of shorter lifetime, but still of significant spectral weight at ε_F , thus maintaining a large Fermi volume up to $T \gtrsim T_K^{(\text{high})} \gg T_K^*$.

by different reflex delay times. Employing this, we showed that at high temperatures $T \approx T_K^{(\text{high})} \gg T_K^*$ the Fermi volume is enlarged by the CEF excitations, both in the Fermi liquid phase (CeCu_6) and in the quantum-critical compound $\text{CeCu}_{5.9}\text{Au}_{0.1}$. At low temperatures $T < \Delta_1$, the large Fermi volume is carried by the ground-state Kondo band in CeCu_6 , but collapses at the QPT [18]. This reconciles, within a single experiment, the existence of a large Fermi volume at $T \gg T_K^*$ with vanishing Kondo weight at the QPT. Since this CEF-induced mechanism appears to be generic, we expect similar behavior of other Ce- and Yb-based heavy-fermion compounds [8, 10, 35, 36] in forthcoming terahertz experiments.

The authors gratefully acknowledge insightful discussions with S. Kirchner, K. Kliemt, C. Krellner, K. Matho, S. Wirth, and G. Zwicky. M. F. thanks CEMS at RIKEN for support of his research sabbatical. This work was financially supported by the Swiss National Science Foundation (SNSF) via Projects No. 200021_147080 (M.F., C.W.) and 200021_178825 (M.F., S.P.) and by the Deutsche Forschungsgemeinschaft (DFG) via Grant No. SFB/TR 185-C4 (J.K., F.Z.).

* manfred.fiebig@mat.ethz.ch

† kroha@physik.uni-bonn.de

- [1] H. v. Löhneysen, A. Rosch, M. Vojta, and P. Wölfle, Fermi-liquid instabilities at magnetic quantum phase transitions, *Rev. Mod. Phys.* **79**, 1015 (2007).
- [2] A. C. Hewson, *The Kondo problem to heavy fermions* (Cambridge University Press, Cambridge, England, 1993).
- [3] A. Benlagra, T. Pruschke, and M. Vojta, Finite-temperature spectra and quasiparticle interference in Kondo lattices: From light electrons to coherent heavy quasiparticles, *Phys. Rev. B* **84**, 195141 (2011).
- [4] H. C. Choi, B. I. Min, J. H. Shim, K. Haule, and G. Kotliar, Temperature-Dependent Fermi Surface Evolution in Heavy Fermion CeIrIn_5 , *Phys. Rev. Lett.* **108**, 016402 (2012).
- [5] P. Coleman, C. Pépin, Q. Si, and R. Ramazashvili, How do Fermi liquids get heavy and die?, *J. Phys. Condens. Matter* **13**, R723 (2001).
- [6] A. Hackl and M. Vojta, Kondo volume collapse, Kondo breakdown, and Fermi surface transitions in heavy-fermion metals, *Phys. Rev. B* **77**, 134439 (2008).
- [7] S. Friedemann, N. Oelscher, S. Wirth, C. Krellner, C. Geibel, F. Steglich, S. Paschen, S. Kirchner, and Q. Si, Fermi surface collapse and dynamical scaling near a quantum-critical point, *Proc. Natl. Acad. Sci. U.S.A.* **107**, 14547 (2010).
- [8] K. Kummer, S. Patil, A. Chikina, M. Güttler, M. Höpner, A. Generalov, S. Danzenbächer, S. Seiro, A. Hannaske, C. Krellner, Yu. Kucherenko, M. Shi, M. Radovic, E. Rienks, G. Zwicky, K. Matho, J. W. Allen, C. Laubschat, C. Geibel, and D. V. Vyalikh, Temperature-Independent Fermi Surface in the Kondo Lattice YbRh_2Si_2 , *Phys. Rev. X* **5**, 011028 (2015).
- [9] S. Paschen, S. Friedemann, S. Wirth, F. Steglich, S. Kirchner, and Q. Si, Kondo destruction in heavy fermion quantum criticality and the photoemission spectrum of YbRh_2Si_2 , *J. Magn. Magn. Mater.* **400**, 17 (2016).
- [10] Q. Y. Chen, D. F. Xu, X. H. Niu, J. Jiang, R. Peng, H. C. Xu, C. H. P. Wen, Z. F. Ding, K. Huang, L. Shu, Y. J. Zhang, H. Lee, V. N. Strocov, M. Shi, F. Bisti, T. Schmitt, Y. B. Huang, P. Dudin, X. C. Lai, S. Kirchner, H. Q. Yuan, and D. L. Feng, Direct observation of how the heavy-fermion state develops in CeCoIn_5 , *Phys. Rev. B* **96**, 045107 (2017).
- [11] J. A. Hertz, Quantum critical phenomena, *Phys. Rev. B* **14**, 1165 (1976).
- [12] T. Moriya, *Spin Fluctuations in Itinerant Electron Magnetism* (Springer, Berlin, 1985).
- [13] A. Millis, Effect of a nonzero temperature on quantum critical points in itinerant fermion systems, *Phys. Rev. B* **48**, 7183 (1993).
- [14] Q. Si, S. Rabello, K. Ingersent and J. L. Smith, Locally critical quantum phase transitions in strongly correlated metals, *Nature (London)* **413**, 804 (2001).
- [15] T. Senthil, M. Vojta and S. Sachdev, Weak magnetism and non-Fermi liquids near heavy-fermion critical points, *Phys. Rev. B* **69**, 035111 (2004).
- [16] P. Wölfle and E. Abrahams, Quasiparticles beyond the Fermi liquid and heavy fermion criticality, *Phys. Rev. B* **84**, 041101(R) (2011).
- [17] A. Nejati, K. Ballmann, and J. Kroha, Kondo Destruction in RKKY-Coupled Kondo Lattice and Multi-Impurity Systems, *Phys. Rev. Lett.* **118**, 117204 (2017).
- [18] C. Wetli, S. Pal, J. Kroha, K. Kliemt, C. Krellner, O. Stockert, H. v. Löhneysen, and M. Fiebig, Time-resolved collapse and revival of the Kondo state near a quantum phase transition, *Nat. Phys.* **14**, 1103 (2018).
- [19] F. Reinert, D. Ehm, S. Schmidt, G. Nicolay, and S. Hüfner, J. Kroha, O. Trovarelli and C. Geibel, Temperature Dependence of the Kondo Resonance and its Satellites in CeCu_2Si_2 , *Phys. Rev. Lett.* **87**, 106401 (2001).
- [20] D. Ehm, S. Schmidt, S. Hüfner, F. Reinert, J. Kroha, P. Wölfle, O. Stockert, C. Geibel and H. von Löhneysen, High resolution photoemission study on low- T_K Ce systems: Kondo resonance, crystal field structures, and their temperature dependence, *Phys. Rev. B* **76**, 045117 (2007).
- [21] M. Klein, A. Nuber, F. Reinert, J. Kroha, O. Stockert, and H. v. Löhneysen, Signature of Quantum Criticality in Photoemission Spectroscopy, *Phys. Rev. Lett.* **101**, 266404 (2008).
- [22] S. Ernst, S. Kirchner, C. Krellner, C. Geibel, G. Zwicky, F. Steglich, and S. Wirth, Emerging local Kondo screening and spatial coherence in the heavy-fermion metal YbRh_2Si_2 , *Nature (London)* **474**, 362 (2011).
- [23] M. Haze, R. Peters, Y. Torii, T. Suematsu, D. Sano, M. Naritsuka, Y. Kasahara, T. Shibauchi, T. Terashima, and Y. Matsuda, Direct Evidence for the Existence of Heavy Quasiparticles in the Magnetically Ordered Phase of CeRhIn_5 , *J. Phys. Soc. Jpn.* **88**, 014706 (2019).
- [24] J. Kroha, S. Kirchner, G. Sellier, P. Wölfle, D. Ehm, F. Reinert, S. Hüfner, and C. Geibel, Structure and transport in multi-orbital Kondo systems, *Physica (Amsterdam)* **18E**, 69 (2003).
- [25] J. R. Schrieffer and P. A. Wolff, Relation between the Anderson and Kondo Hamiltonians, *Phys. Rev.* **149**, 491 (1966).
- [26] F. Zamani, P. Ribeiro, and S. Kirchner, The functional integral formulation of the Schrieffer-Wolff transformation, *New J. Phys.* **18**, 063024 (2016).
- [27] B. Stroka, A. Schröder, T. Trappmann, H. v. Löhneysen, M. Loewenhaupt, and A. Severing, Crystal-field excitations in the heavy-fermion alloys $\text{CeCu}_{6-x}\text{Au}_x$ studied by specific

- heat and inelastic neutron scattering, *Z. Phys. B* **90**, 155 (1993).
- [28] E. A. Goremychkin and R. Osborn, Neutron-spectroscopy study of the heavy-fermion compound CeCu_6 , *Phys. Rev. B* **47**, 14580 (1993).
- [29] U. Witte, R. Schedler, O. Stockert, and M. Loewenhaupt, The investigation of the crystalline electric field of CeCu_2 and CeCu_6 , *J. Low Temp. Phys.* **147**, 97 (2007).
- [30] See Supplemental Material at <http://link.aps.org/supplemental/...> for the geometry of the experimental setup, details of the multiorbital Anderson lattice model and its parameter values, and of the DMFT calculations, which includes Refs. [31, 32].
- [31] T. A. Costi, J. Kroha, and P. Wölfle, Spectral properties of the Anderson impurity model: Comparison of numerical renormalization group and noncrossing approximation results, *Phys. Rev. B* **53**, 1850 (1996).
- [32] J. Kroha and P. Wölfle, Conserving Diagrammatic Approximations for Quantum Impurity Models: NCA and CTMA, *J. Phys. Soc. Jpn.* **74**, 16 (2005).
- [33] When the conduction band has holelike character (negative dispersion), its hybridization with the heavy Ce states leads to a decrease of the Fermi momentum, as discussed in [34] for the holelike compound CeRhIn_5 . This is consistent with our present findings of a Kondo-induced Fermi momentum increase, since the hole number counts negative.
- [34] Q. Y. Chen, D. F. Xu, X. H. Niu, R. Peng, H. C. Xu, C. H. P. Wen, X. Liu, L. Shu, S. Y. Tan, X. C. Lai, Y. J. Zhang, H. Lee, V. N. Strocov, F. Bisti, P. Dudin, J.-X. Zhu, H. Q. Yuan, S. Kirchner, and D. L. Feng, Band Dependent Interlayer f -Electron Hybridization in CeRhIn_5 , *Phys. Rev. Lett.* **120**, 066403 (2018).
- [35] S. Jang, J. D. Denlinger, J. W. Allen, V. S. Zapf, M. B. Maple, J. N. Kim, B. G. Jang, and J. H. Shim, Evolution of the Kondo lattice electronic structure above the transport coherence temperature, arXiv:1704.08247.
- [36] A. Generalov, J. Falke, I. A. Nechaev, M. M. Otrokov, M. Güttler, A. Chikina, K. Kliemt, S. Seiro, K. Kummer, S. Danzenbächer, D. Usachov, T. K. Kim, P. Dudin, E. V. Chulkov, C. Laubschat, C. Geibel, C. Krellner, and D. V. Vyalikh, Strong spin-orbit coupling in the noncentrosymmetric Kondo lattice, *Phys. Rev. B* **98**, 115157 (2018).

Supplemental Material for Fermi volume evolution and crystal field excitations in heavy-fermion compounds probed by time-domain terahertz spectroscopy

S. Pal¹, C. Wetli¹, F. Zamani², O. Stockert³, H. v. Löhneysen⁴, M. Fiebig¹, J. Kroha^{2,5}

¹ Department of Materials, ETH Zürich, 8093 Zürich, Switzerland

² Physikalisches Institut and Bethe Center for Theoretical Physics, Universität Bonn, Nussallee 12, 53115 Bonn, Germany

³ Max Planck Institute for Chemical Physics of Solids, 01187 Dresden, Germany

⁴ Institut für Festkörperphysik and Physikalisches Institut, Karlsruhe Institute of Technology, 76021 Karlsruhe

⁵ Center for Correlated Matter, Zhejiang University, Hangzhou, Zhejiang 310058, China

This supplement describes specifications of the experimental setup as well as the definition of the multi-orbital Anderson lattice model and details of the dynamical mean-field theory (DMFT) calculations with the non-crossing approximation (NCA) as the impurity solver.

Terahertz time domain reflection spectroscopy

Geometry of experimental setup. The terahertz time domain spectroscopy is performed in reflection geometry. All $\text{CeCu}_{6-x}\text{Au}_x$ samples were cut from single crystals of orthorhombic crystal structure, and faces perpendicular to the crystallographic c -axis were polished using SiC. The samples were then mounted in a temperature-controlled Janis SVT-400 helium reservoir cryostat such that the c axis is parallel to the plane of the optical table. Linearly polarized terahertz radiation with a spectral range of 0.1–3 THz was incident on the sample at an angle of 45° , the terahertz electric field E_{THz} oriented perpendicular to the crystallographic a axis, see Fig. S1. Hence, E_{THz} is P-polarized, i.e., parallel to the plane of incidence.

THz pulse generation and analysis. Single-cycle terahertz pulses of a few nanojoules are generated by optical rectification in a 0.5 mm ZnTe-(110) single crystal, using 90 % of a Ti:Sapphire laser output (wavelength 800 nm, pulse duration 120 fs, pulse repetition rate 1 kHz, 2 mJ per pulse). The remaining 10 % of the fundamental 800

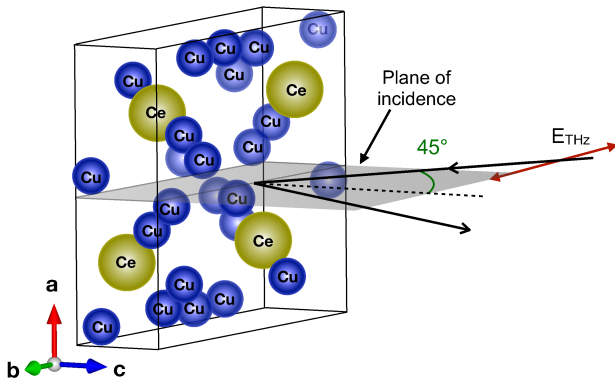


Figure S1. The crystallographic axes of the sample and experimental geometry using P-polarized light, with a 45° incidence angle.

nm laser pulse are used as a probe (or gating) pulse for the electrooptic sampling of the reflected terahertz wave. The terahertz and the gating beams are collinearly focused onto a ZnTe-(110) detection crystal. The terahertz-induced ellipticity of the probe light is measured using a quarter-wave plate, a Wollaston polarizer and a balanced photodiode (BPD). The signal from the BPD is then analyzed with a lock-in amplifier. In order to increase the accessible time delay between the terahertz and the probe pulses, Fabry-Pérot resonances from the faces of the 0.5 mm thick ZnTe-(110) crystal are suppressed by extending the detection-crystal with a 2-mm-thick, terahertz-inactive ZnTe-(100) crystal that is optically bonded to the back of the detection crystal.

Multi-orbital Anderson lattice model

In the orthorhombic lattice structure of $\text{CeCu}_{6-x}\text{Au}_x$, the fourteen (including spin) orbitals of the Ce 4f shell are split by spin-orbit coupling into a total angular momentum $j = 5/2$ ground-state multiplet and a $j = 7/2$ excited multiplet, with a spin orbit splitting of $\Delta_{SO} \approx 250$ meV [1]. The ground-state multiplet is further split by the crystal electric field (CEF) into three Kramers doublets with excitation energies $\Delta_m^{(0)} = \varepsilon_m - \varepsilon_0$, $m = 1, 2$, above the ground-state energy ε_0 , see Fig. 1 of the main article. The $\text{CeCu}_{6-x}\text{Au}_x$ system with the three low-lying Ce 4f Kramers doublets accessible by thermal or terahertz excitation is, thus, described by the Anderson lattice model with three local orbitals,

$$\begin{aligned}
 H = & \sum_{\mathbf{k}, \sigma} \varepsilon_{\mathbf{k}} c_{\mathbf{k}\sigma}^\dagger c_{\mathbf{k}\sigma} + \sum_{i, m, \sigma} \varepsilon_m d_{im\sigma}^\dagger d_{im\sigma} \\
 & + \frac{U}{2} \sum_{i, (m, \sigma) \neq (m', \sigma')} d_{im\sigma}^\dagger d_{im\sigma} d_{im'\sigma'}^\dagger d_{im'\sigma'} \\
 & + \sum_{\mathbf{k}, i, m, \sigma} \left(V_{\mathbf{k}m} e^{-i\mathbf{k}\mathbf{r}_i} c_{\mathbf{k}\sigma}^\dagger d_{im\sigma} + V_{m\mathbf{k}}^* e^{i\mathbf{k}\mathbf{r}_i} d_{im\sigma}^\dagger c_{\mathbf{k}\sigma} \right), \quad (\text{S1})
 \end{aligned}$$

where $c_{\mathbf{k}\sigma}^\dagger, c_{\mathbf{k}\sigma}$ are the field operators for conduction electrons in momentum and spin state $|\mathbf{k}, \sigma\rangle$ with dispersion $\varepsilon_{\mathbf{k}}$. $d_{im\sigma}^\dagger, d_{im\sigma}$ are the operators for electrons in the Ce 4f Kramers doublet states $|m, \sigma\rangle$ located at the lattice sites i , with single-particle binding energies ε_m , $m = 0, 1, 2$, $\sigma = \pm 1/2$. The third term of the Hamiltonian represents the strong Coulomb repulsion U between electrons in any of the Ce 4f orbitals which effectively enforces single occupancy of the Ce 4f shell in accordance with the valence of the cerium atoms in $\text{CeCu}_{6-x}\text{Au}_x$. For the calculations we, therefore, take $U \rightarrow \infty$. The fourth term describes the hybridization between the conduction electron states and the Ce 4f states $|m, \sigma\rangle$ on each lattice site i . We apply standard dynamical mean-field theory (DMFT) to compute the energy- and momentum-dependent spectral functions of the hybridizing (light) conduction band and the three CEF-split 4f bands of this interacting system, shown in Fig. 5 of the main article. As the DMFT impurity solver we use the multi-orbital generalization of the slave-boson (SB) representation within the non-crossing approximation (NCA) [1, 2], because it is able to describe the spectra over the complete width of the uncorrelated conduction band of $O(10 \text{ eV})$, while maintaining a resolution of better than $O(0.1 \text{ meV})$ near the Fermi level, necessary to resolve all CEF resonances at low temperatures $T < T_K^*$. For a single Anderson impurity in the $U \rightarrow \infty$ limit, the NCA is known to correctly describe the width and temperature dependence of the Kondo and CEF spectral features from high T down to well below T_K^* [1, 2].

In the SB formulation, each quantum state $|m, \sigma\rangle$ of the Ce 4f shell on site i is represented by a fermionic field $f_{im\sigma}^\dagger$ and the unoccupied Ce 4f shell by a bosonic field b_i^\dagger , such that the electron operators read $d_{im\sigma}^\dagger = f_{im\sigma}^\dagger b_i$, with the local operator constraint $\sum_{m\sigma} f_{im\sigma}^\dagger f_{im\sigma} + b_i^\dagger b_i = 1$. The local (retarded) pseudofermion propagator $G_{fmm'\sigma}(\omega)$ and its selfenergy $\Sigma_{fmm'\sigma}(\omega)$ are nondiagonal matrices in Ce 4f orbital space,

$$G_{fmm'\sigma}(\omega) = [(\omega - \lambda - \varepsilon_m)\delta_{mm'} - \Sigma_{fmm'\sigma}(\omega)]^{-1}, \quad (\text{S2})$$

and the (retarded) slave boson propagator reads,

$$G_b(\omega) = (\omega - \lambda - \Sigma_b(\omega))^{-1}. \quad (\text{S3})$$

λ is a chemical-potential parameter used to enforce the constraint exactly by the limit $\lambda \rightarrow \infty$ at the end of the calculation [2]. The multi-orbital NCA equations then read [3],

$$\Sigma_{fmm'\sigma}(\omega) = \Gamma_{mm'} \int d\varepsilon f(\varepsilon) \tilde{A}_{c\sigma}(-\varepsilon) G_b(\omega + \varepsilon) \quad (\text{S4})$$

$$\Sigma_b(\omega) = \sum_{mm'\sigma} \Gamma_{m'm} \int d\varepsilon f(\varepsilon) \tilde{A}_{c\sigma}(\varepsilon) G_{fmm'\sigma}(\omega + \varepsilon). \quad (\text{S5})$$

Here, $f(\varepsilon)$ is the Fermi distribution function, $\tilde{A}_{c\sigma}(\varepsilon)$ the momentum-integrated c -electron spectral density without

scattering from the DMFT impurity site, and

$$\Gamma_{mm'} = \sum_{\mathbf{k}} V_{m\mathbf{k}}^* |\text{Im} G_{c\mathbf{k}\sigma}^{(0)}(0)| V_{\mathbf{k}m'} \quad (\text{S6})$$

is the effective hybridization matrix, with $G_{c\mathbf{k}\sigma}^{(0)}(0)$ the bare c -electron propagator at the Fermi energy. The NCA equations (S4), (S5) together with Eqs. (S2), (S3) are solved selfconsistently by iteration. See [2] for an efficient numerical treatment. Denoting the slave-boson and pseudofermion spectral functions by $A_b(\varepsilon) = -\text{Im} G_b(\varepsilon)/\pi$ and $A_{fmm'\sigma}(\varepsilon) = -\text{Im} G_{fmm'\sigma}(\varepsilon)/\pi$, respectively, the Green's function for electrons in the Ce 4f orbitals is then obtained as ($\beta = 1/(k_B T)$)

$$G_{dmm'\sigma}(\omega) = \int d\varepsilon e^{-\beta\varepsilon} [G_{fmm'\sigma}(\omega + \varepsilon) A_b(\varepsilon) - A_{fmm'\sigma}(\varepsilon) G_b(\varepsilon - \omega)], \quad (\text{S7})$$

which is subsequently fed into the DMFT loop.

For the numerical evaluations we considered, for simplicity, a three-dimensional, cubic tight-binding lattice. The parameter values (in units of the bare conduction half bandwidth D , where for copper $D \approx 8 \text{ eV}$) were adjusted as

$$\begin{aligned} \varepsilon_0 &= -0.5, & \varepsilon_1 &= -0.499, & \varepsilon_2 &= -0.0498 \\ \Gamma_{00} &= 0.063, & \Gamma_{11} &= 0.042, & \Gamma_{22} &= 0.032, \\ \Gamma_{01} &= 0.0053, & \Gamma_{12} &= 0.0105, & \Gamma_{02} &= 0.0053 \end{aligned}$$

These values reproduce the experimentally known values for CeCu_6 of $T_K^* \approx 6 \text{ K}$ and CEF splittings $\Delta_1 = 7 \text{ meV}$, $\Delta_2 = 13 \text{ meV}$ [4–6].

* manfred.fiebig@mat.ethz.ch

† kroha@physik.uni-bonn.de

- [1] D. Ehm, S. Schmidt, S. Hühner, F. Reinert, J. Kroha, P. Wölfle, O. Stockert, C. Geibel and H. von Löhneysen, High resolution photoemission study on low- T_K Ce systems: Kondo resonance, crystal field structures, and their temperature dependence, Phys. Rev. B **76**, 045117 (2007).
- [2] T. A. Costi, J. Kroha, and P. Wölfle, Spectral properties of the Anderson impurity model: Comparison of numerical renormalization group and non-crossing approximation results, Phys. Rev. B **53**, 1850 (1996).
- [3] J. Kroha and P. Wölfle, Conserving Diagrammatic Approximations for Quantum Impurity Models: NCA and CTMA, J. Phys. Soc. Japan **74**, 16 (2005).
- [4] B. Stroka, A. Schröder, T. Trappmann, H. v. Löhneysen, M. Loewenhaupt, and A. Severing, Crystal-field excitations in the heavy-fermion alloys $\text{CeCu}_{6-x}\text{Au}_x$ studied by specific heat and inelastic neutron scattering, Z. Phys. B **90**, 155 (1993).
- [5] E. A. Goremychkin and R. Osborn, Neutron-spectroscopy study of the heavy-fermion compound CeCu_6 , Phys. Rev. B **47**, 14580 (1993).
- [6] U. Witte, R. Schedler, O. Stockert, and M. Loewenhaupt, The investigation of the crystalline electric field of CeCu_2 and CeCu_6 , J. Low Temp. Phys. **147**, 97 (2007).